

Initial state fluctuations from mid-peripheral to ultra-central collisions in an event-by-event transport approach

S. Plumari,^{1,2} G. L. Guardo,^{1,2} F. Scardina,^{1,2} and V. Greco^{1,2}

¹*Department of Physics and Astronomy, University of Catania, Via S. Sofia 64, I-95125 Catania*

²*INFN-Laboratori Nazionali del Sud, Via S. Sofia 62, I-95123 Catania, Italy*

We have developed a relativistic kinetic transport approach that incorporates initial state fluctuations allowing to study the build up of elliptic flow v_2 and high order harmonics v_3 , v_4 and v_5 for a fluid at fixed $\eta/s(T)$. We study the effect of the η/s ratio and its T dependence on the build up of the $v_n(p_T)$ for two different beam energies: RHIC for Au+Au at $\sqrt{s} = 200 \text{ GeV}$ and LHC for Pb + Pb at $\sqrt{s} = 2.76 \text{ TeV}$. We find that for the two different beam energies considered the suppression of the $v_n(p_T)$ due to the viscosity of the medium have different contributions coming from the cross over or QGP phase. Our study reveals that only in ultra-central collisions (0 – 0.2%) the $v_n(p_T)$ have a stronger sensitivity to the T dependence of η/s in the QGP phase and this sensitivity increases with the order of the harmonic n. Moreover, the study of the correlations between the initial spatial anisotropies ϵ_n and the final flow coefficients v_n shows that at LHC energies there is more correlation than at RHIC energies. The degree of correlation increases from peripheral to central collisions, but only in ultra-central collisions at LHC, we find that the linear correlation coefficient $C(n, n) \approx 1$ for $n = 2, 3, 4$ and 5. This suggests that the final correlations in the (v_n, v_m) space reflect the initial correlations in the (ϵ_n, ϵ_m) space.

PACS numbers: 12.38.Aw, 12.38.Mh

Keywords: Heavy ion collisions, Shear Viscosity, Elliptic Flow, Transport Theory, Initial state fluctuations.

I. INTRODUCTION

The experimental results accumulated in these years in the ultra relativistic heavy ion collisions (uRHICs) first in the experiments conducted at RHIC and more recently at the LHC has shown that the elliptic flow $v_2 = \langle \cos(2\varphi_p) \rangle = \langle (p_x^2 - p_y^2) / (p_x^2 + p_y^2) \rangle$, is the largest ever observed in HIC [1, 2]. The elliptic flow is a measurement of the momentum anisotropy of the emitted particles and it is an observable that encodes information about the transport properties of the matter created in these collisions. Theoretical calculations within viscous hydrodynamics [3, 4] and in the recent years also calculation performed within transport approach [5–7] have shown that this large value of v_2 is consistent with a matter with a very low shear viscosity to entropy density ratio η/s close to the conjectured lower bound for a strongly interacting system, $\eta/s = 1/4\pi$ [8].

While early studies have been focused on elliptic flow generated by the global almond shape of the fireball for non central collisions. In the recent years the possibility to measure experimentally the event-by-event angular distribution of emitted particle has made possible to go beyond such a simplified picture accessing the fluctuating shape that encodes higher order harmonics generating non zero flows $v_n = \langle \cos(n\varphi_p) \rangle$ [9–11]. Hence most of the research activity has been now focused on the study of the effects of the fluctuations in the initial geometry due to the fluctuations of the position of the nucleons in the overlap region of the collision [12–17]. Such fluctuations in the initial geometry are sources for momentum anisotropies of any n-th order harmonics $v_n = \langle \cos(n\varphi_p) \rangle$ and in particular of the triangular flow $n = 3$, that especially in ultra-central collisions appears

as the largest one [11, 18, 19].

The comparison between event-by-event viscous hydrodynamical calculations and the experimental results for v_n seems to confirm a finite but not too large value of $4\pi\eta/s \sim 1 - 3$ [15, 16]. However, small values of η/s is not an evidence of the creation of a QGP phase. A phenomenological estimation of its temperature dependence could give information if the matter created in these collisions undergoes a phase transition [20–22]. Information about a temperature dependence of η/s can be achieved studying the $v_2(p_T)$ and the high order harmonic $v_n(p_T)$ in a wider range of energies. Similar studies have been performed using a transport approach but only for the elliptic flow in an approach not incorporating event-by-event fluctuations [22, 23]. In this paper we extend this analysis to high order harmonics studying the role of the η/s on the build up of $v_n(p_T)$ using for the first time a cascade approach with initial state fluctuations.

There are several theoretical indications that η/s should have a particular behavior with the temperature [20, 21, 24–27]. As an example in Fig.1 it is shown a collection of theoretical results about the temperature dependence of η/s . Fig.1 shows that in general η/s should have a typical behavior of phase transition with a minimum close to the critical temperature T_C [20–23]. On one hand at low temperature estimates of η/s in the chiral perturbation theory for a meson gas [24, 25], have shown that in general η/s is a decreasing function with the temperature, see down-triangles in Fig.1. Similar results for η/s have been extrapolated from heavy-ion collisions at intermediate energies, see HIC-IE diamonds in Fig.1. On the other hand at higher temperature $T > T_c$ lQCD calculation have shown that in general η/s becomes an increasing function with the temperature [26, 29], see up-

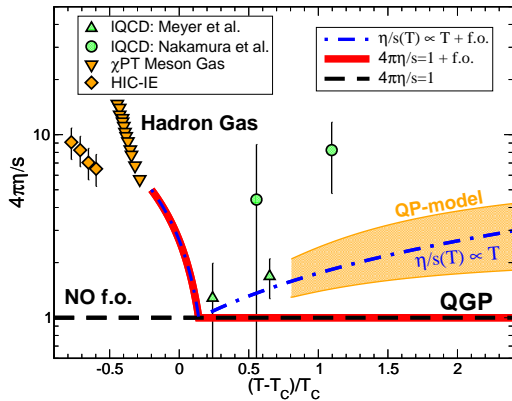


FIG. 1: Different parametrizations for η/s as a function of the temperature. The orange area refers to the quasi-particle model predictions for η/s [28]. The three different lines indicate different possible T dependencies studied in this paper. Symbols are as in the legend. See the text for more details.

triangles and circles in Fig.1, but due to the large error bars in the IQCD results for η/s it is not possible to infer a clear temperature dependence in the QGP phase. The analysis at different energies of $v_2(p_T)$ and the extension to high order harmonics $v_n(p_T)$ can give further information about the T dependence of η/s . In this paper we study and discuss the build-up of anisotropic flows v_n in ultra-relativistic HIC treating the system as a fluid with some $\eta/s(T)$. This is achieved by mean of a transport approach with initial state fluctuations. The paper is organized as follows. In Section II, we introduce the transport approach at fixed shear viscosity to entropy density η/s . In Section III, we discuss the initial conditions and in particular the implementation of the initial state fluctuations in the transport approach. In Section IV, we study the time evolution of the anisotropic flows $\langle v_n \rangle$ and the effect of the $\eta/s(T)$ on the differential $v_n(p_T)$. Finally in Section V we study the correlations between the initial asymmetry in coordinate space measured by the coefficients ϵ_n and the final anisotropy in momentum space measured by the anisotropic flows $\langle v_n \rangle$. In this paper we will show results on $v_n(p_T)$ for $n = 2, 3, 4$ and 5 for the two different systems $Au + Au$ at $\sqrt{s} = 200$ GeV and $Pb + Pb$ at $\sqrt{s} = 2.76$ TeV at different centralities.

II. KINETIC APPROACH AT FIXED SHEAR VISCOSITY TO ENTROPY DENSITY RATIO

In this work we employ the kinetic transport theory to study the evolution of the fireball created in relativistic heavy-ion collisions. We perform such simulations using a relativistic transport code developed in these years to perform studies of the dynamics of heavy-ion collisions at both RHIC and LHC energies [5, 7, 30–33]. The evolution of the phase-space distribution function $f(x, p, t)$ is given by solving the Relativistic Boltzmann Transport (RBT)

equation:

$$p^\mu \partial_\mu f(x, p) = C[f] + S[f_0] \quad (1)$$

where $C[f]$ is the Boltzmann-like collision integral. In the result shown in this paper we have considered only the $2 \leftrightarrow 2$ processes and for one component system $C[f]$ can be written as,

$$C[f] = \int_{2,1',2'} (f_{1'} f_{2'} - f f_2) |\mathcal{M}|^2 \delta^4(p + p_2 - p_{1'} - p_{2'}) \quad (2)$$

where $\int_{2,1',2'} = \int \Pi_{k=2,1',2'} d^3 p_k / 2E_k (2\pi)^3$ and \mathcal{M} denotes the transition amplitude for the elastic processes which is directly linked to the differential cross section $|\mathcal{M}|^2 = 16\pi s (s - 4M^2) d\sigma/dt$ with s the Mandelstam invariant. Numerically we solve the RBT equation using the so called test particle method and the collision integral is solved by using Monte Carlo methods based on the stochastic interpretation of transition amplitude [5, 31, 34].

In the standard use of the transport theory one fixes the microscopical details of the scattering like matrix element or cross sections of the processes to study the effect of the microscopical details on the observables. This is however not our aim we exploit the cross section σ_{tot} as a tool to determine the η/s of the system. As shown in [35] in the hydrodynamic limit observables like $v_2(p_T)$ or spectra don't depend on the microscopic details encoded in $|\mathcal{M}|^2$. In agreement with the implicit assumption of hydrodynamics. In such an approach it is possible to study directly the impact of η/s on observables like the anisotropic flows $v_n(p_T)$ which is the main focus of this paper. Compared with the viscous hydrodynamic calculations a kinetic approach at fixed η/s has many two advantages: first in this approach we start from a description in terms of $f(x, p)$ instead of starting from $T^{\mu\nu}(x)$ and it is possible to include initial non equilibrium effects (see [32, 33]). Second, this approach is not based on an ansatz for the viscous corrections for the phase-space distribution function δf with the limitation in the transverse momentum range in order to ensure that $\delta f/f \ll 1$. Also this approach provides a tool to study the effect of η/s on the observables in a wider range of η/s and in transverse momentum p_T . Notice also that the kinetic freeze-out can be determined self-consistently with an increasing $\eta/s(T)$ that determines a smooth switching-off of the scattering rates. A more detailed discussion can be found in previous papers, see [5, 32, 33]. The disadvantage of the present approach is that hadronization has not yet been included. A more general disadvantage is that RBT converge to viscous hydrodynamics with the relaxation time typical of a kinetic theory. However viscous hydrodynamics with relaxation times of kinetic theory have been shown to be in quite good agreement with experimental data.

In order to study the dynamical evolution of the fireball with a certain $\eta/s(T)$ we determine locally in space and time the total cross section σ_{tot} needed to have the

wanted local viscosity. As shown in [31] the Chapman-Enskog theory correctly describes the relation between $\eta \leftrightarrow T, \sigma(\theta), \rho$ providing a good agreement with the results obtained using the Green-Kubo correlator. In the Chapman-Enskog theory and for a pQCD inspired cross section, typically used in parton cascade approaches [5, 6, 34, 36–39], $d\sigma/dt \sim \alpha_s^2/(t - m_D^2)^2$, the η/s is given by the following expression:

$$\eta/s = \frac{1}{15} \langle p \rangle \tau_\eta = \frac{1}{15} \frac{\langle p \rangle}{g(a) \sigma_{tot} \rho}, \quad (3)$$

where $a = m_D/2T$, with m_D being the screening mass regulating the angular dependence of the cross section, while $g(a)$ is the proper function accounting for the pertinent relaxation time $\tau_\eta^{-1} = g(a) \sigma_{tot} \rho$ associated to the shear transport coefficient and it is given by:

$$g(a) = \frac{1}{50} \int dy y^6 \left[\left(y^2 + \frac{1}{3} \right) K_3(2y) - y K_2(2y) \right] h \left(\frac{a^2}{y^2} \right), \quad (4)$$

where K_n -s are the Bessel functions and the function h relate the transport cross section to the total cross section $\sigma_{tr}(s) = \sigma_{tot} h(m_D^2/s)$ with $h(\zeta) = 4\zeta(1+\zeta)[(2\zeta+1)\ln(1+1/\zeta) - 2]$.

In order to study the role of the η/s ratio and its temperature dependence we consider three different cases: one with a constant $4\pi\eta/s = 1$ during all the evolution of the system dashed line in Fig.1 another one with $4\pi\eta/s = 1$ at higher temperature in the QGP phase and an increasing η/s in the cross over region towards the estimated value for hadronic matter $4\pi\eta/s \approx 6$ [25, 40] shown by solid line in Fig.1. Such an increase of η/s in the cross over region $0.8T_C \leq T \leq 1.2T_C$ allows for a smooth realistic realization of the kinetic freeze-out. This is because at lower temperature, according to the formula Eq.(3) $\sigma \propto (\eta/s)^{-1}$ i.e. the increase of η/s towards the estimated value for the hadronic matter implies the total cross section decrease and this permits to achieve in a self-consistent way the kinetic freeze-out. In the following discussion the term f.o. means to take into account the increase of η/s at low temperature. The third one is shown in Fig.1 by the dot dashed line. In this case we consider the increase of η/s at higher temperature with a linear temperature dependence and a minimum close to the critical temperature with a temperature dependence similar to that expected from general considerations as shown in Fig.1.

III. INITIAL CONDITIONS

The main novelty in the present paper is the implementation of initial state fluctuations in a transport cascade approach. We will consider two systems at different centralities: $Au + Au$ collisions at $\sqrt{s_{NN}} = 200 \text{ GeV}$ produced at RHIC and $Pb + Pb$ collisions at $\sqrt{s_{NN}} = 2.76 \text{ TeV}$ at LHC. In particular in this section we discuss the implementation of the initial state fluctuations

in the above transport approach. In order to generate an event by event initial profile we use the Monte-Carlo Glauber model. In this model the Woods-Saxon distribution is used to sample randomly the positions of the nucleons in the two colliding nucleus A and B . In this way a discrete distribution for these nucleons is generated. We employ the geometrical method to determine if the two nucleons one from the nucleus A and the other one from the nucleus B are colliding. Within this method two nucleons collide each other if the relative distance in the transverse plane is $d_T \leq \sqrt{\sigma_{NN}/\pi}$ where σ_{NN} is the nucleon-nucleon cross section. In our calculation we have used $\sigma_{NN} = 4.2 \text{ fm}^2$ for RHIC and $\sigma_{NN} = 7.0 \text{ fm}^2$ for LHC. N_{coll} and N_{part} are given by counting the number of collisions and the number of participating nucleons for each event. The next step is the conversion of the discrete distribution for the nucleons into a smooth one by assuming for each nucleon a gaussian distribution centered in the nucleon position. In our model we choose to convert the information of the nucleon distribution into the density in the transverse plane $\rho_T(x, y)$ which is given by the following sum

$$\rho_T(x, y) = C \sum_{i=1}^{N_{part}} \exp \left[- \frac{(x - x_i)^2 + (y - y_i)^2}{2\sigma_{xy}^2} \right] \quad (5)$$

where C is an overall normalization factor fixed by the longitudinal distribution dN/dy while σ_{xy} is the Gaussian width which regulates the smearing of the fluctuations and in the following calculations it has been fixed to $\sigma_{xy} = 0.5 \text{ fm}$. In our calculation we have assumed initially a longitudinal boost invariant distribution from $y = -2.5$ to $y = 2.5$. In the first column of Fig.2 it is shown the contour plot of the initial transverse density at mid rapidity for a given event with impact parameter $b = 7.5 \text{ fm}$. The upper panel refers to the system $Au + Au$ at $\sqrt{s_{NN}} = 200 \text{ GeV}$ and the lower panel to $Pb + Pb$ at $\sqrt{s_{NN}} = 2.76 \text{ TeV}$.

The transverse density $\rho_T(x, y)$ fixes the initial anisotropy in coordinate space that is quantified in terms of the following coefficients ϵ_n :

$$\epsilon_n = \frac{\sqrt{\langle r_T^n \cos(n\phi) \rangle^2 + \langle r_T^n \sin(n\phi) \rangle^2}}{\langle r_T^n \rangle} \quad (6)$$

where $r_T = \sqrt{x^2 + y^2}$ and $\phi = \arctan(y/x)$ is the polar coordinate in the transverse plane. In Fig.3 it is shown the initial spatial anisotropies $\epsilon_2, \epsilon_3, \epsilon_4$ and ϵ_5 as a function of the impact parameter. The second coefficient ϵ_2 shows a stronger dependence with the impact parameter with respect to the other coefficients because it acquires a contribution due to the global almond shape of the fireball while the other harmonics have most of their origin in the fluctuations of the positions of the nucleons. For more central collisions $b \leq 2.5 \text{ fm}$ the ϵ_2 is even smaller than the other harmonics because when the effect of the elliptic overlap region disappears it becomes more difficult to have fluctuations of the positions of the nucleons along only one preferential direction.

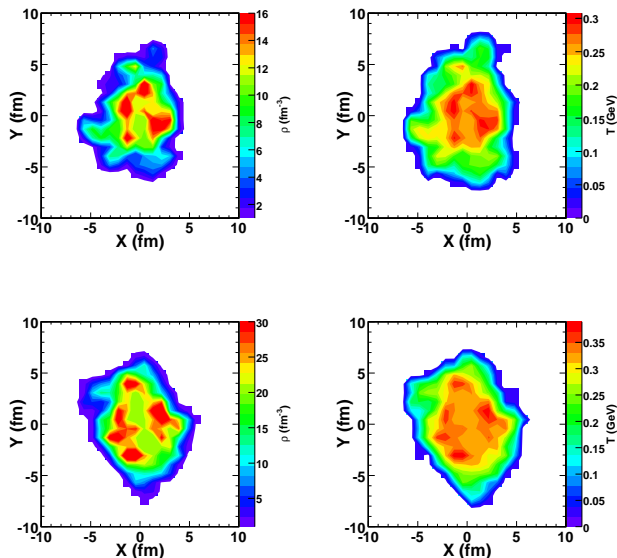


FIG. 2: In the left column it is shown the initial transverse density $\rho_T(x, y)$ at mid rapidity for two typical events for $Au + Au$ at $\sqrt{s_{NN}} = 200 \text{ GeV}$ (upper panel) and $Pb + Pb$ at $\sqrt{s_{NN}} = 2.76 \text{ TeV}$ (lower panel). In the right column it is shown the corresponding initial temperature in transverse plane. These plots are for an impact parameter of $b = 7.5 \text{ fm}$.

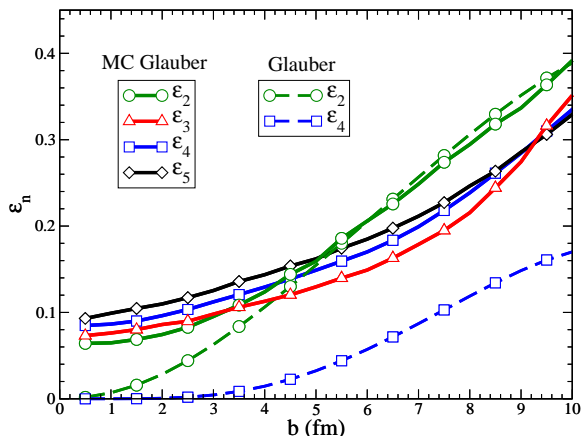


FIG. 3: Initial spatial anisotropies ϵ_n as a function of the impact parameter. Different symbols are for different n . The solid lines refer to the Monte Carlo Glauber while the dashed ones to the optical Glauber model.

For the initialization in momentum space at RHIC (LHC) energies we have considered for partons with transverse momentum $p_T \leq p_0 = 2 \text{ GeV}$ (3 GeV) a thermalized spectrum in the transverse plane. Assuming the local equilibrium the initial local temperature in the transverse plane $T(x, y)$ is evaluated by using the standard thermodynamical relation $\rho_T(x, y) = \gamma T^3 / \pi^2$

with $\gamma = 2 \times (N_c^2 - 1) + 2 \times 2 \times N_c \times N_f = 40$ with $N_c = 3$ and $N_f = 2$. In the right column of Fig.2 it is shown the corresponding initial local temperature in transverse plane. As shown in the central region of the fireball for mid peripheral collision we can reach temperature $T \approx 300 \text{ MeV}$ at RHIC and $T \approx 400 \text{ MeV}$ at LHC. While for partons with $p_T > p_0$ we have assumed the spectrum of non-quenched minijets according to standard NLO-pQCD calculations with a power law shape [41, 42]. In coordinate space the partons with $p_T > p_0$ have been distributed according the binary collisions. The initial transverse momentum of the particles is distributed uniformly in the azimuthal angle. We fix the initial time of the simulation to $\tau_0 = 0.6 \text{ fm}/c$ for RHIC and $\tau_0 = 0.3 \text{ fm}/c$ for LHC.

In the following discussion, we will consider two different types of initial conditions. One consisting in a fixed initial distribution by using the standard Glauber model as used in previous works, see [5, 7, 22, 30]. The second one consisting of an initial profile changing event by event according to the MC Glauber model as discussed before.

In our simulations we have used $N_{event} = 500$ events for each centrality class. This number is enough to get solid results for the spectra, differential elliptic flow and high order flow coefficients $v_n(p_t)$. For the study of the correlations between the initial ϵ_n and the final v_n that will be shown in the next section we have extended this analysis to 10^3 events. The inclusion of the initial state fluctuations introduce a further difficulties because in order to get stable results we need to have a good sampling of the initial geometry event by event and this is controlled by the total number of test particles N_{test} . Furthermore an irregular initial profile need a good calculation grid resolution. We have checked the convergency of our results for v_2, v_3 and v_4 with the lattice spacing of the calculation grid and N_{test} . We found the convergency for a grid with a transverse area of the cell $A_T = 0.12 \text{ fm}^2$ and $N_{test} = 2 \cdot 10^6$ as total number of test particles per event.

The elliptic flow $v_2(p_T)$ and the high order harmonics $v_3(p_t)$, $v_4(p_T)$ and $v_5(p_T)$ have been calculated as

$$v_n = \langle \cos [n(\phi - \Psi_n)] \rangle \quad (7)$$

where the momentum space angles Ψ_n are given by

$$\Psi_n = \frac{1}{n} \arctan \frac{\langle \sin(n\phi) \rangle}{\langle \cos(n\phi) \rangle} \quad (8)$$

In this section first we discuss the comparison between the Glauber model w/o initial fluctuations with the MC Glauber with fluctuations. Without initial state fluctuations only even harmonics can be generated therefore we will consider here only $v_2(p_T)$ and $v_4(p_T)$. In the left panel of Fig.4 we compare the differential elliptic flow $v_2(p_T)$ obtained with an initial state that changes event by event according to the MC Glauber model (solid lines) as discussed in details the previous section with the

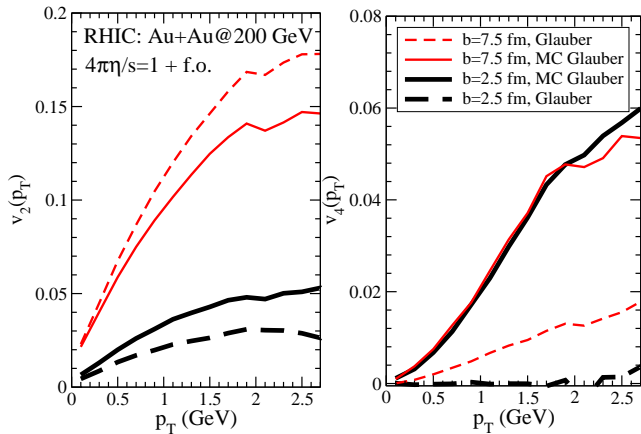


FIG. 4: Results for $Au + Au$ collisions at $\sqrt{s_{NN}} = 200 \text{ GeV}$ for mid rapidity. Left: differential elliptic flow $v_2(p_T)$ at mid rapidity. The solid lines refer to the case with initial state fluctuations the dashed lines are for the case without initial fluctuations. Thick lines are for $b = 2.5 \text{ fm}$ while thin lines for $b = 7.5 \text{ fm}$. Right: differential $v_4(p_T)$ at mid rapidity with the same legend as in the left panel.

one obtained for the case with an averaged initial profile (dashed lines). These results are for $Au + Au$ collisions at $\sqrt{s} = 200 \text{ GeV}$ and for 20 – 30% centrality class. In these calculations we have considered $4\pi\eta/s = 1$ at high temperature and an increasing η/s at lower temperature as shown by the red solid line in Fig.1. As shown for mid peripheral collision (with $b = 7.5 \text{ fm}$) the effect of the fluctuations in the initial geometry is to reduce the $v_2(p_T)$ of about 15%, despite the same initial eccentricity ϵ_2 in Glauber and MC Glauber, see green solid and dashed lines in Fig.3. The reduced efficiency in building up the $v_2(p_T)$ is related to the fact that for an irregular geometry in the transverse plane the pressure gradients generate also a small counter-flow towards the inner part of the fireball reducing the azimuthal anisotropy in momentum space due to the global almond shape. The introduction of the fluctuations in the initial geometry play the role to generate the higher order harmonics in particular the odd harmonics which were absent by symmetry in the averaged initial configuration. In the right panel of Fig.4 we show the same comparison for the quadrangular flow $v_4(p_T)$. We observe an opposite behaviour: the initial state fluctuations increase the final $v_4(p_T)$ by a factor of 3. This result is related to the fact that the fluctuations introduce about a factor 3 larger initial ϵ_4 as shown by the comparison between blue solid and dashed lines in Fig.3. In other words for mid peripheral collisions most of $v_2(p_T)$ comes from the global almond shape while $v_4(p_T)$ comes normally from the initial fluctuations. In fact as shown by the black thick solid and dashed lines in the left panel of Fig.3 the effect of the fluctuations is to produce a larger $v_2(p_T)$. From the comparison between thick black solid and dashed line in the right panel of Fig.3 we observe a non zero $v_4(p_T)$ that was absent in the averaged

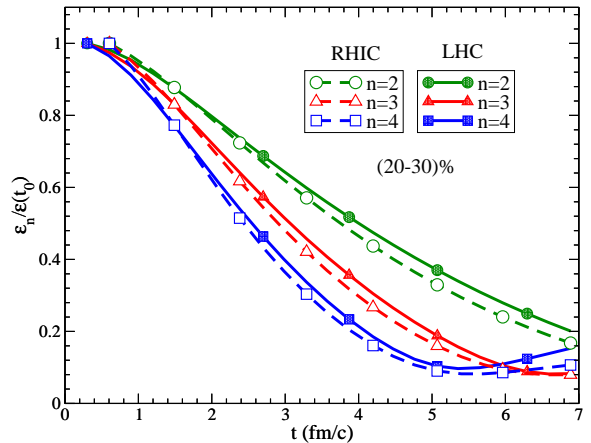


FIG. 5: $\epsilon_n/\epsilon_n(t_0)$ as a function of the time for $Au + Au$ collisions at $\sqrt{s_{NN}} = 200 \text{ GeV}$ (dashed lines) and for $Pb + Pb$ collisions at $\sqrt{s_{NN}} = 2.76 \text{ TeV}$ (solid lines). Different symbols refer to different harmonics n .

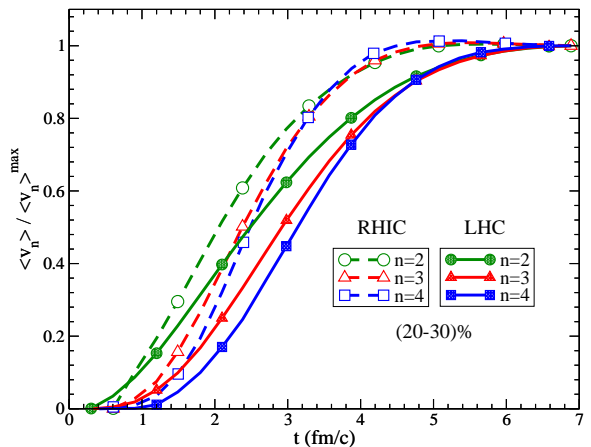


FIG. 6: $\langle v_n \rangle / \langle v_n \rangle^{max}$ as a function of time at mid rapidity and for (20 – 30)% of centrality. Dashed lines are the results for $Au + Au$ at $\sqrt{s_{NN}} = 200 \text{ GeV}$ while solid lines $Pb + Pb$ at $\sqrt{s_{NN}} = 2.76 \text{ TeV}$. Different symbols correspond to different harmonics.

initial profile where the initial $\epsilon_4 \approx 0$ (see blue dashed line in Fig.3). Moreover we observe a low sensitivity of $v_4(p_T)$ with the centrality similarly to the experimental data at RHIC energies [10]. Such a behaviour would be impossible to explain without initial state fluctuations.

IV. EFFECTS OF $\eta/s(T)$ ON THE $v_n(p_T)$

In the first part of this section we discuss the time evolution of the eccentricities ϵ_n and the anisotropic flow coefficients $\langle v_n \rangle$ for $Au + Au$ collisions at $\sqrt{s} = 200 \text{ GeV}$ (solid lines) and for $Pb + Pb$ collisions at $\sqrt{s} = 2.76 \text{ TeV}$ In Fig.5 we plot the time evolution of the ϵ_n normalized

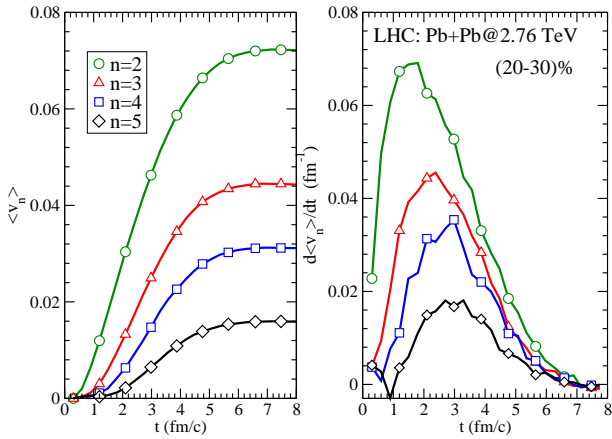


FIG. 7: Left panel: time evolution of $\langle v_n \rangle$ at mid rapidity respectively for (20 – 30)% centrality collisions. Different symbols are for different harmonics. Right panel: Production rate $\frac{d\langle v_n \rangle}{dt}$ as a function of time at mid rapidity and for the same centrality. These results are for $Pb + Pb$ collision at $\sqrt{s_{NN}} = 2.76 \text{ TeV}$.

to the initial eccentricity $\epsilon_n(t_0 = 0.6 \text{ fm}/c)$ for RHIC and $\epsilon_n(t_0 = 0.3 \text{ fm}/c)$ for LHC. At very early times the small deformation of the fireball in the transverse plane decrease linearly with time and at first order of this deformation we have that $\epsilon_n \propto \epsilon_n(t_0) - \alpha_n t^{n-2}$. This gives the ordering in the time evolution of ϵ_n shown in Fig.5. the time evolution of ϵ_n is faster for larger n .

On contrary v_n show an opposite behaviour during the early times of the expansion of the fireball. In Fig.6 it shown the average $\langle v_n \rangle$ normalized to its maximum value at the end of the expansion. The $\langle v_n \rangle$ appear later for larger n and their development is flatter at early times for larger n . Similar results have been obtained in a $2 + 1D$ transport approach where considerations on the early times evolution of the fireball give that $\langle v_n \rangle \propto t^n$ [43, 44]. As shown in left panel of Fig.7 we observe that in the time evolution of the different harmonics $\langle v_n \rangle$ the ordering is present also at late times. In right panel of Fig.7 it is shown the production rate for the different harmonics and as shown different harmonics have different production rates. In particular, we observe that at very early time the second harmonic has a non zero value for $\frac{d\langle v_2 \rangle}{dt} \neq 0$ at variance with higher harmonics for which $\frac{d\langle v_n \rangle}{dt} \approx 0$. This different behaviour could be the origin of the stronger correlation between the final elliptic flow v_2 and its initial eccentricity ϵ_2 that becomes weaker between the final v_n and the initial ϵ_n for higher harmonics ($n > 2$), see Section V.

Differential flow coefficients $v_n(p_T)$ are observables that carry out more information about the fireball created in the heavy ion collisions in particular because they are sensitive to the transport properties of the medium like the η/s ratio. In the following discussion we will study the effect of the η/s on the build up of the ellip-

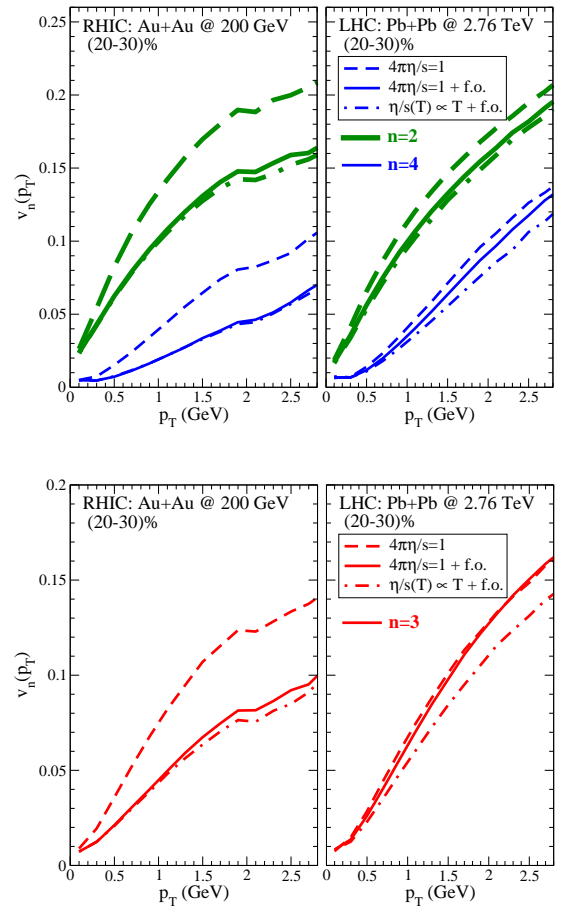


FIG. 8: Upper panel: differential $v_2(p_T)$ (thick lines) and $v_4(p_T)$ (thin lines) green and blue lines respectively at mid rapidity and for (20 – 30)% collision centrality. The comparison is between the two systems: $Au + Au$ at $\sqrt{s} = 200 \text{ GeV}$ (left) and $Pb + Pb$ at $\sqrt{s} = 2.76 \text{ TeV}$ (right). The dashed lines refer to the case with a constant $\eta/s = (4\pi)^{-1}$ during all the evolution. The solid lines refer to the case with $\eta/s = (4\pi)^{-1}$ at higher temperature and with an increasing η/s ratio at lower temperature while the dot dashed lines to the case with $\eta/s \propto T$ at higher temperature and with an increasing η/s ratio at lower temperature. Right panel: differential $v_3(p_T)$ in red lines with the same legend as in the upper panel.

tic flow $v_2(p_T)$ and on the high order harmonics $v_3(p_T)$, $v_4(p_T)$ and $v_5(p_T)$. With $v_n(p_T)$ we mean the root mean square $\sqrt{\langle v_n^2 \rangle}$ as it has been done in experimental data using the event plane method. In the upper panel of Fig.8 it is shown the elliptic flow $v_2(p_T)$ (green thick lines) and the $v_4(p_T)$ (blue thin lines) at mid rapidity and for (20 – 30)% centrality for both RHIC $Au + Au$ at $\sqrt{s} = 200 \text{ GeV}$ (left panel) and LHC $Pb + Pb$ at $\sqrt{s} = 2.76 \text{ TeV}$ (right panel). In general in agreement with what has been obtained in viscous hydrodynamical calculations, the increase of the viscosity of the medium has the effect to reduce both v_2 and v_4 .

As we can see at RHIC energies comparing the thick dashed lines with the solid ones, in the left panel of Fig.8,

the $v_2(p_T)$ is sensitive to the increase of the η/s at lower temperature close to the cross over region. In particular the effect is a reduction of the elliptic flow of about 17%. A similar trend were observed for the 4-th harmonic $v_4(p_T)$ where we have a reduction due to the increase of η/s at lower temperature but the effect in this case is about a factor two larger then the previous one, i.e. about 30 – 40%. The different sensitivity to the η/s can be attributed to their different formation time, $t_{v_4} > t_{v_2}$ [38]. As shown in Fig.6 each harmonics v_n start to develop at different times. In particular v_4 has its maximum development approximatively at $\tau \approx 3 fm/c$ while the v_2 at $\tau \approx 1.2 fm/c$. This means that different harmonics probe mainly different temperatures and different value of the η/s ratio. Assuming that the first few fm/c of the expanding fireball are dominated by the 1D longitudinal expansion [32] where approximatively $T(\tau) = T_0(\tau_0/\tau)^{1/3}$ we have that when v_4 has its maximum development at about $\tau \approx 3 fm/c$ the temperature is $1.3T_C$ at RHIC and $2T_C$ at LHC. In other words this tell us that v_4 at RHIC energies mainly develops closer to the cross over region where η/s should increase.

On the other hand at LHC energies, left panel of Fig.8, the scenario is different, the elliptic flow is almost unaffected by the increase of η/s ratio at low temperature (in the hadronic phase) as we can see comparing the green thick dashed line with the solid one. Instead we observe that the increase of η/s at lower temperature has a more sensitive effect on the $v_4(p_T)$ with a reduction of about 5–10%, see blue solid and dashed lines. Again this different sensitivity to the η/s in the cross over region between v_2 and v_4 at LHC are consistent with the results obtained at RHIC energies and depends on the different formation time of the harmonics in relation to the initial T of the system. The greater sensitivity at RHIC energies of both v_2 and v_4 to the η/s at low temperature is related to the different life time of the fireball. In fact the life time of the fireball at LHC is greater than that at RHIC, 8-10 fm/c at LHC against 4-5 fm/c at RHIC. In general this means that at RHIC energies the v_n have not enough time to fully develop in the QGP phase. While at LHC energies we have that the v_n develops almost completely in the QGP phase and therefore it is less sensitive to the dynamics in the cross-over and hadronic region. This result were firstly found w/o initial state fluctuation in refs.[7, 30, 45] but remain similar also with fluctuations. The last however allow to study for the first time a similar effect also on $v_3(p_T)$.

In Fig.8 it is shown the effect of an $\eta/s(T)$ in the QGP phase. In the comparison between the solid lines and the dot dashed ones the only difference is in the linear temperature dependence of $\eta/s \propto T$ for $T > T_C$ while at lower temperature we have the same dependence (see dot dashed lines in Fig.1). As we can see the v_4 at LHC is sensitive to the change of η/s at higher temperature while at RHIC energies the v_4 is completely unaffected by this change. In the lower panel of Fig.8 it is shown the triangular flow $v_3(p_T)$ (red lines) at mid rapidity for

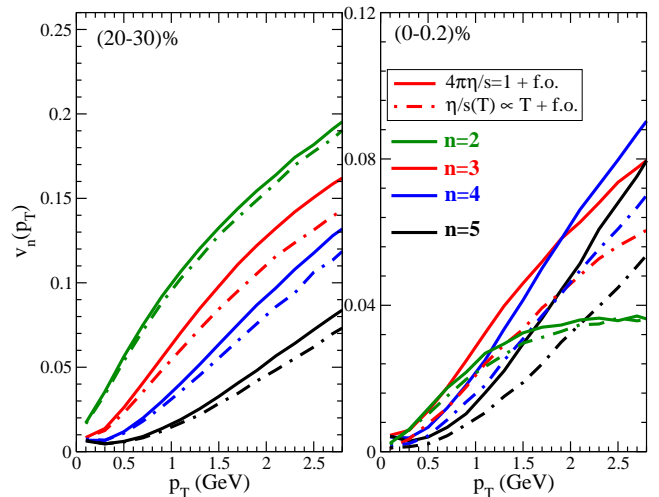


FIG. 9: Comparison between $v_n(p_T)$ for mid-peripheral (left panel) and central (right panel) collision. Different colors refer to different harmonics while solid lines correspond to $4\pi\eta/s = 1$ in QGP phase and f.o. and dot dashed lines to $\eta/s \propto T$ in the QGP phase and f.o.

(20–30)% centrality and for both RHIC $Au+Au$ at $\sqrt{s} = 200 GeV$ (left panel) and LHC $Pb+Pb$ at $\sqrt{s} = 2.76 TeV$ (right panel). In agreement with what has been obtained for the even harmonics v_2 and v_4 , we observe at RHIC energies a reduction of $v_3(p_T)$ due to the increase of the η/s at low temperature with a reduction of about 25%, while at LHC it is almost insensitive to the change of η/s in the cross over region. However we observe that at LHC the third and fourth harmonics are more sensitive to the change of $\eta/s(T)$ with respect to the elliptic flow with a deviation of about 10% for v_3 and v_4 against a less 5% for v_2 . Still it has be noted that such a sensitivity is quite small to hoping a determination of the T dependence of η/s from the $v_n(p_T)$.

Very recently it has been possible to access also experimentally to the ultra-central collisions. The ultra-central collisions are interesting because the initial ϵ_n come completely from the fluctuations in the initial geometry rather than by global geometric overlap region. In Fig.9 it is shown the comparison of $v_n(p_T)$ produced in $Pb + Pb$ at $\sqrt{s} = 2.76 TeV$ collisions for different centralities: left panel for mid-peripheral collisions and right panel for central collisions. Different colors are for different harmonics. Solid lines refer to the case with $\eta/s = 1/(4\pi)$ in the QGP phase and the increase at low temperature as shown in Fig.1 by red solid lines while the dot-dashed lines refer to the case with $\eta/s \propto T$ in the QGP phase and the increase at low temperature as shown in Fig.1 by blue dot dashed lines. From the comparison we observe that at low p_T both centralities the $v_n(p_T)$ are much flatter for larger n . This results is in agreement with that obtained in hydrodynamic calculations where $v_n(p_T) \propto p_T^n$ [46]. On the other hand at high p_T for ultra-central collisions we observe that the

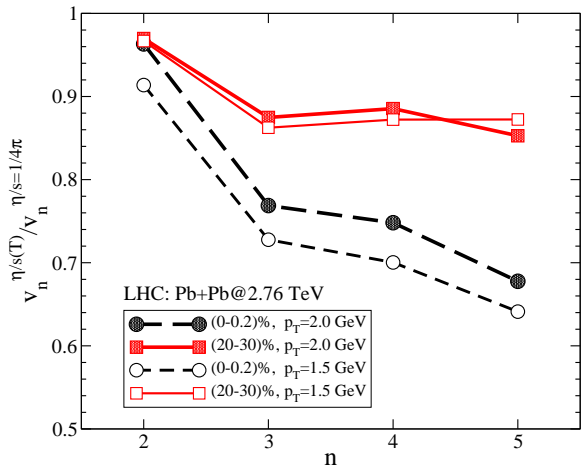


FIG. 10: Ratio between $v_n(p_T)$ for two different parametrizations of η/s as a function of the order of the harmonic n and for $p_T = 1.5\text{GeV}$ (open symbols) and $p_T = 2\text{GeV}$ (full symbols). Solid lines refer to mid peripheral collisions while dashed lines to ultra-central collisions.

elliptic flow $v_2(p_T)$ shows a saturation while for $n \geq 3$ $v_n(p_T)$ increase linearly with p_T . This is in qualitative agreement with what has been observed experimentally, but a quantitative comparison would require the inclusion of hadronization that however would not affect the sensitivity to $\eta/s(T)$. In particular the sensitivity to the value of η/s in the QGP phase increase with the increasing the order of the harmonics n in agreement with the fact that viscous corrections to $v_n(p_T)$ increase with the harmonics [35]. Furthermore we observe that reduction of $v_n(p_T)$ due to the increase of η/s in the QGP phase (dot dashed lines) is strongly enhanced for ultra-central collisions. As shown in Fig.10 for $n \geq 3$ the reduction for central collisions is about 30 – 35% against a reduction of about 10% for mid peripheral collisions. It is indeed remarkable that a 30% effect is determined by a slowly linear rising of η/s with T as the one considered and depicted in Fig.1. In particular in central collisions higher harmonics acquire a larger sensitivity to the value of the viscosity in the QGP phase. Therefore our study suggest that to have information about $\eta/s(T)$ one should focus on ultra-central collisions. This point is further strenghtened by the study of the correlations between v_n and the initial eccentricities ϵ_n that we discuss in the next section.

V. CORRELATIONS BETWEEN v_n AND ϵ_n

In recent years, the correlation between integrated v_2 and high order harmonics v_3, v_4 with the initial asymmetry in coordinate space ϵ_2, ϵ_3 and ϵ_4 have been studied in the event-by-event ideal and viscous hydrodynamics framework [47–49]. In general it has been shown that the elliptic flow is strongly correlated with initial eccentric-

ity while a weaker correlation has been found for higher harmonics v_3, v_4 with ϵ_3 and ϵ_4 . One explanation for the weak correlation observed between v_4 and ϵ_4 is that for final v_4 there is also a correlation with the initial ϵ_2 . In particular in [47] has been shown that it possible to have a good linear correlation between v_4 and a linear combination of the initial ϵ_2 and ϵ_4 .

In this section we discuss these correlations within an event by event transport approach with initial state fluctuations. A measure of the linear correlation is given by the correlation coefficient $C(n, m)$ given by the following expression:

$$C(n, m) = \frac{\sum_i (\epsilon_n^i - \langle \epsilon_n \rangle) (v_m^i - \langle v_m \rangle)}{\sqrt{\sum_i (\epsilon_n^i - \langle \epsilon_n \rangle)^2 \sum_i (v_m^i - \langle v_m \rangle)^2}} \quad (9)$$

where ϵ_n^i and v_m^i are the values of ϵ_n and v_m corresponding to the given event i and evaluated according Eq.s (6) and (7). $C(n, m) \approx 1$ corresponds to a strong linear correlation between the initial ϵ_n and the final v_m .

The results shown in this section have been obtained with $N_{event} = 1000$ events for each centrality class a total number of test particle per event $N_{test} = 2 \cdot 10^6$. In Fig.11, it is shown the two-dimensional plots of the integrated flow coefficients v_n as a function of the corresponding initial ϵ_n for each event. The results shown are for $Au + Au$ collisions at $\sqrt{s_{NN}} = 200\text{GeV}$ and for three different centralities (10 – 20)%, (20 – 30)% and (30 – 40)%. The viscosity has been fixed to $4\pi\eta/s = 1$ plus a kinetic f.o. realized by the increase in $\eta/s(T)$ as in Fig.1. As shown in the upper panel we observe a stronger linear correlation between ϵ_2 and v_2 for mid central collisions with a linear correlation coefficient that shows a monotonic behaviour with the collision centrality from $C(2, 2) \approx 0.96$ for (10 – 20)% to $C(2, 2) \approx 0.89$ for (30 – 40)%. Qualitatively the results are in agreement with the one obtained within a 2+1D viscous hydrodynamics, see [49]. In general we observe a slightly smaller degree of correlation probably induced by the fact that we simulate a 3+1D expansion that can be expected to contribute to the decorrelation. In the middle and lower panel of Fig.11 we have shown similar plots for the third and fourth harmonics. We observe again a reduction of the correlation coefficient with the centrality of the collision similarly to v_2 and ϵ_2 . We obtain that the correlation between ϵ_3 and v_3 for all the collision centralities is weaker with respect to that obtained for the elliptic flow. Furthermore the fourth harmonic flow v_4 shows a weak correlation with the initial ϵ_4 in particular for mid-peripheral collisions where the linear correlation coefficient is quite weak $C(4, 4) < 0.3$. Furthermore we observe that the $\langle v_n \rangle / \epsilon_n$ ratio (see dashed lines in Fig.11) decreases when decreases the correlation coefficient $C(n, n)$, i.e. for more peripheral collisions.

A similar behaviour for the linear correlation coefficient $C(n, n)$ is observed at LHC energies for $Pb + Pb$ collisions at $\sqrt{s_{NN}} = 2.76\text{TeV}$. In Fig.12 it is shown the comparison between ultra-central and mid-peripheral

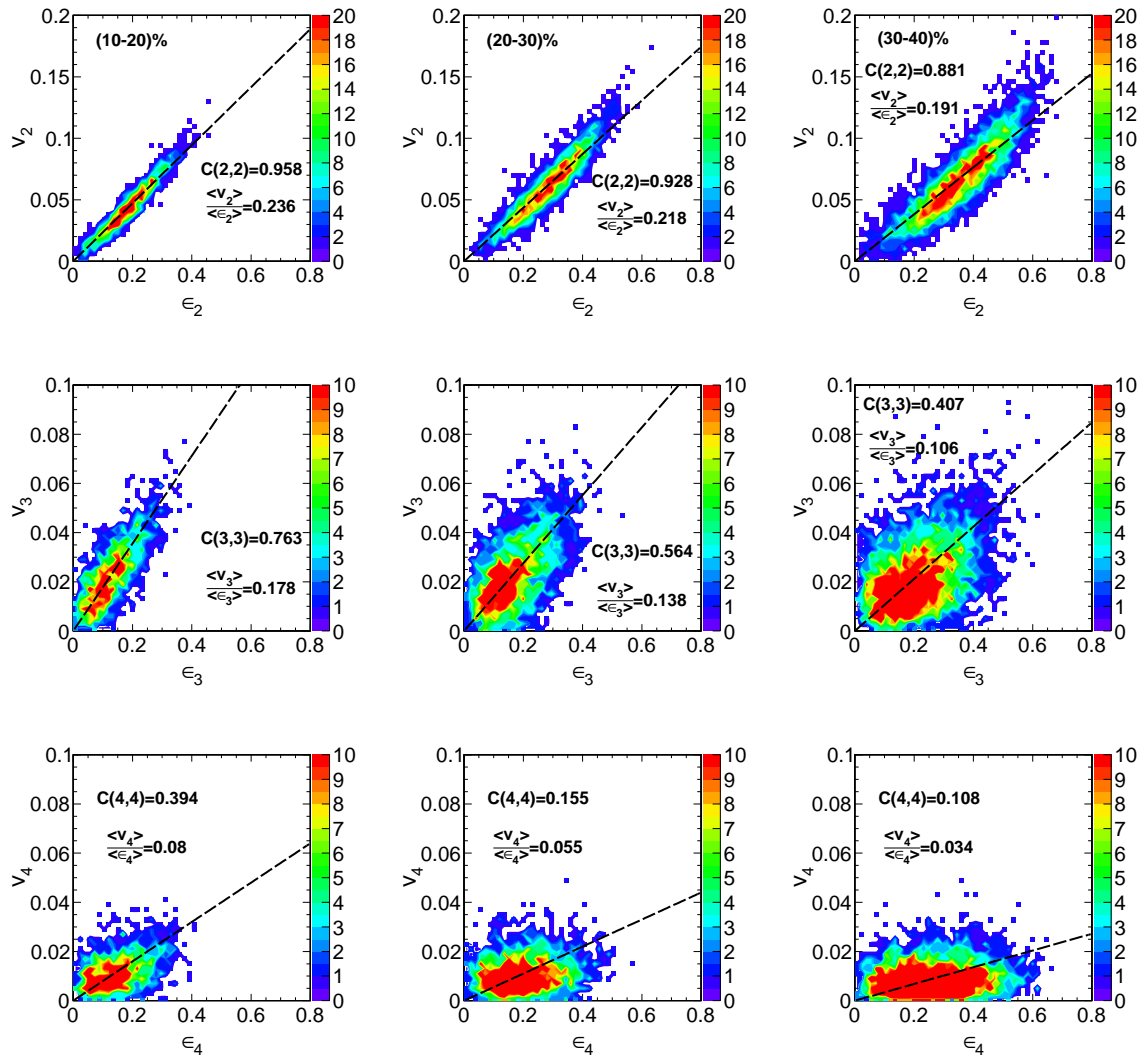


FIG. 11: ϵ_n and v_n for $Au + Au$ collisions at $\sqrt{s_{NN}} = 200 \text{ GeV}$ and for three different centrality class. Upper panel: ϵ_2 and v_2 for (10 – 20)%, (20 – 30)% and (30 – 40)% from left to right. Middle panel: ϵ_3 and v_3 for the same centralities. Finally in the lower panel ϵ_4 and v_4 . In these calculations we have fixed $\eta/s = 1/(4\pi)$ for high temperature and the kinetic f.o. at lower temperature (see solid line in Fig.1).

collision at LHC energies at $\sqrt{s_{NN}} = 2.76 \text{ TeV}$. In ultra-central collisions the $\langle v_n \rangle$ are more correlated to the initial ϵ_n than at peripheral collisions and very interesting differences emerge looking also at higher harmonics.

In order to better visualize and discuss such differences we have plot in Fig.13 the $C(n,n)$ as a function of the impact parameter for both RHIC (dashed lines) and LHC energies (solid lines). As shown the linear correlation coefficient is a decreasing function of the impact parameter for all the harmonics. However, as we can see comparing the dashed and solid lines show, at LHC energies there is a stronger correlation between ϵ_n and v_n for all n with respect to RHIC energies. We observe that v_2 and ϵ_2 have the same degree of correlation for both RHIC and LHC energies while a lower degree of correla-

tion it is shown for higher harmonics $n = 3, 4$ and $n = 5$. More interesting is the fact that for ultra-central collisions at LHC the linear correlation coefficient $C(n,n)$ remains above 0.9 for $n = 2, 3, 4$ and even the $n = 5$ shows large $C(n,n) = 0.85$. This can be visualized also in the right panel of Fig.12 where the (v_n, ϵ_n) correlation plot is shown in mid-peripheral (20 – 30%) collisions (left panel) and in ultra-central collisions (0 – 0.2%) (right panels).

The strong correlation observed for ultra-central collisions means that the value obtained for $\langle v_n \rangle$ and its dependence with the harmonics n for those collisions is strongly related to the value of the initial asymmetry measure ϵ_n . In particular this could imply that the structure of the $v_n(p_T)$ at LHC where $C(n,n) \approx 1$ carry out information about the initial geometry of the fluctuations.

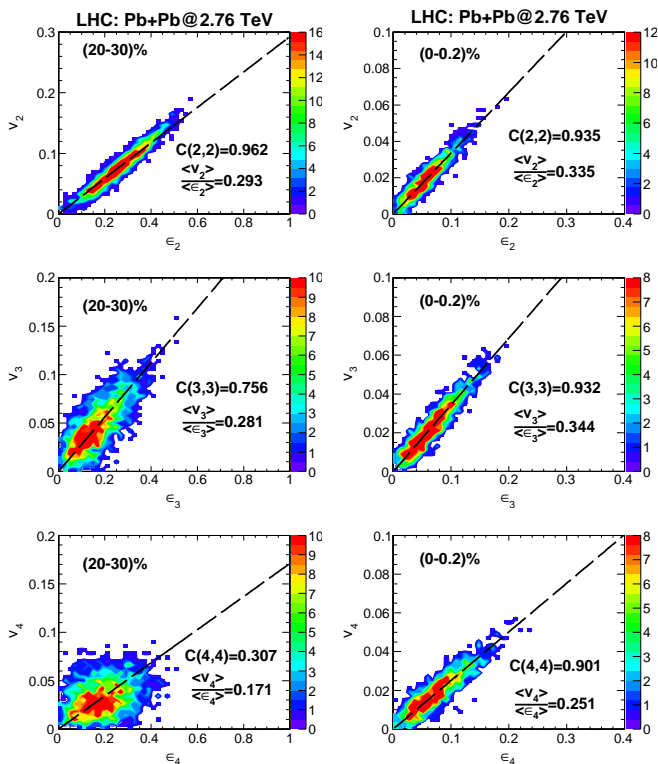


FIG. 12: ϵ_n and v_n for $Pb + Pb$ collisions at $\sqrt{s_{NN}} = 2.76 \text{ TeV}$ and for (20 – 30)% and (0 – 0.2)% centrality cut respectively right and left panel. In these calculations we have fixed $\eta/s = 1/(4\pi)$ for high temperature and the kinetic f.o. at lower temperature (see solid line in Fig.1).

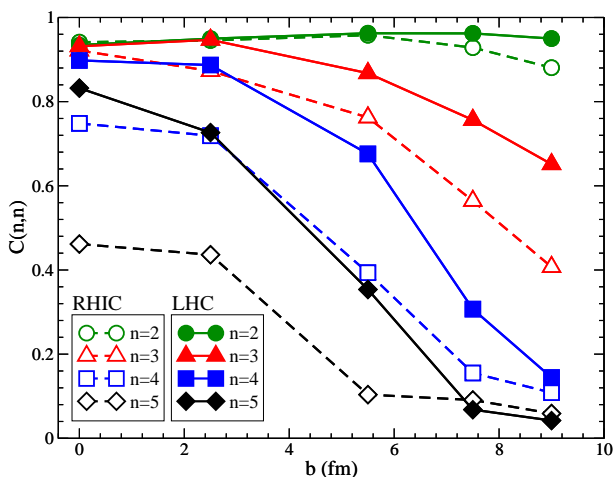


FIG. 13: Correlation coefficient $C(n, n)$ as a function of the impact parameter b . Different symbols refer to different harmonics n . In particular circles, triangles, squares and diamonds refer to $n = 2, 3, 4$ and 5 respectively. The solid lines correspond to $Au + Au$ collisions at $\sqrt{s_{NN}} = 200 \text{ GeV}$ while dashed lines to the system $Pb + Pb$ at $\sqrt{s_{NN}} = 2.76 \text{ TeV}$.

TABLE I: Linear correlation coefficient $C(n, n)$ for RHIC and LHC energies and for different temperature parametrization of η/s . These results are for (20 – 30)% centrality class.

$C(n, n)$	n	$4\pi\eta/s = 1$	$4\pi\eta/s = 1 + \text{f.o.}$	$\eta/s \propto T + \text{f.o.}$
RHIC	2	0.95	0.94	0.93
	3	0.70	0.58	0.65
	4	0.30	0.28	0.31
LHC	2	0.96	0.96	0.96
	3	0.78	0.78	0.74
	4	0.39	0.38	0.38

This joined to the observation that for ultra-central collisions the sensitivity of v_n to η/s is increased by about a factor of 2-3 strongly suggests to focus the experimental efforts at LHC highest energy and ultra-central collisions.

To study the effect of the viscosity and its possible temperature dependence on the correlation we have studied how change the correlation coefficient with the different parametrizations for η/s . In Table I we show the results for $C(n, n)$ for the two energies RHIC and LHC for (20 – 30)% centrality class. In general for this centrality we observe that at LHC energies and for all the viscosities considered the degree of correlation between ϵ_n and v_n is greater than the one at RHIC energies. Moreover we obtain that at LHC the correlation coefficient is not sensitive to the change of the viscosity both at low and high temperature. A slight different behaviour we have at RHIC energies where the effect of the kinetic freeze out is to reduce the degree of correlation between the initial ϵ_n and the final v_n . Furthermore, we have computed the non diagonal components for the linear correlation coefficient $C(n, m)$. We found that $C(2, 3) \approx 0$. and $C(3, 4) \approx 0$ for all the range of centralities explored which means that there is no linear correlation between v_2 and ϵ_3 and v_3 and ϵ_4 . A different behaviour we observe for $C(4, 2)$ which is seen to be an increasing function with the centrality $C(4, 2) \approx 0.02$ for central collision ($b = 0 \text{ fm}$) and about $C(4, 2) \approx 0.23$ at $b = 7.8 \text{ fm}$. This means that in more peripheral collisions the 4th harmonic v_4 has some contamination of ϵ_2 and it is not driven only by ϵ_4 as already suggested in [47].

Some interesting properties of the v_n distributions can be inferred by studying the centrality dependence of the relative fluctuations $\sigma_{v_n}/\langle v_n \rangle$. In Fig.14a) it is shown the $\langle N_{part} \rangle$ dependence of the ratios $\sigma_{v_n}/\langle v_n \rangle$ and $\sigma_{\epsilon_n}/\langle \epsilon_n \rangle$ where σ_{v_n} and σ_{ϵ_n} are the standard deviation respectively for v_n and ϵ_n . As shown for $n = 2$ we observe a strong dependence of the relative fluctuations with the centrality of the collision with $\sigma_{v_2}/\langle v_2 \rangle \approx 0.4$ for $\langle N_{part} \rangle \approx 130$. For more central collisions this ratio approaches the value expected for a 2D Gaussian distribution where $\sigma_{v_n}/\langle v_n \rangle = \sqrt{4/\pi - 1} \approx 0.523$ [50], shown by dashed line in Fig.14. For higher harmonic $n = 3, 4$ and 5 as shown from Fig.14b) to Fig.14d) the values of

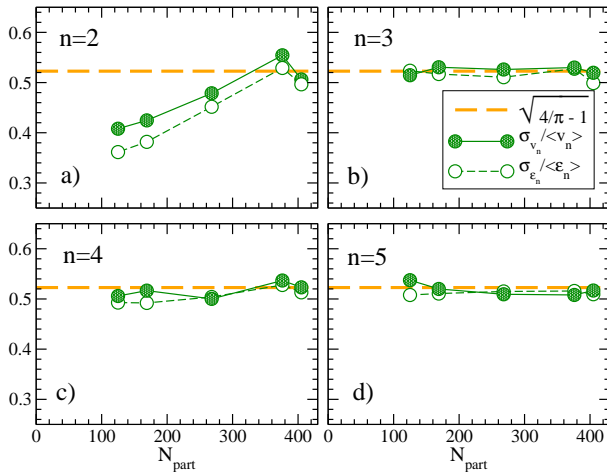


FIG. 14: From panel a) to d) $\sigma_{v_n}/\langle v_n \rangle$ (full symbols) and $\sigma_{\epsilon_n}/\langle \epsilon_n \rangle$ (open symbols) as a function of $\langle N_{part} \rangle$ respectively for $n = 2, 3, 4$ and 5 . The dashed lines indicate the value $\sqrt{4/\pi - 1}$ expected for a 2D Gaussian distribution. These results are for $Pb + Pb$ collisions at $\sqrt{s_{NN}} = 2.76 TeV$.

$\sigma_{v_n}/\langle v_n \rangle$ are approximately the same of the ones of the initial geometry with $\sigma_{v_n}/\langle v_n \rangle \approx \sigma_{\epsilon_n}/\langle \epsilon_n \rangle$ and they are almost independent of the collision centrality and for all the centralities studied they are very close to the value $\sqrt{4/\pi - 1}$ shown by the dashed lines. These results imply that the distributions of v_3, v_4 and v_5 for all the centrality range studied are consistent with the fluctuation-only scenario discussed in [50] and these fluctuations are related to the fluctuations of the initial geometry. On the other hand, the distribution of v_2 is close to this limit for most central collisions while for mid-peripheral collisions there is a contribution coming from the global average geometry.

VI. CONCLUSIONS

Using an event-by-event transport approach we have investigated the build up of the anisotropic flows $v_n(p_T)$ for $n = 2, 3, 4$ and 5 . In particular we have studied the effect of η/s ratio on $v_n(p_T)$ for two different beam energies: at RHIC for $Au + Au$ collisions at $\sqrt{s} = 200 GeV$

and at LHC for $Pb + Pb$ collisions at $\sqrt{s} = 2.76 TeV$. We have found that at RHIC the $v_n(p_T)$ are more affected by the value of η/s at low temperature ($T < 1.2T_C$) and the sensitivity increases with the order of the harmonics. At LHC we get a different effect, all the $v_n(p_T)$ develop in the QGP phase at and are not affected by the value of η/s in the cross-over region. However the sensitivity to the T dependence of the η/s is quite weak, more specifically a constant $\eta/s = 0.08$ or an $\eta/s \propto T$ induce differences in the v_2 of at most a 5% and of about a 10% in v_3, v_4, v_5 . The novel result from our analysis is that such a scenario changes for ultra-central collisions where found an enhancement of the sensitivity of the $v_n(p_T)$ that for $n = 3, 4, 5$ reaches about a 30%. We have also studied the correlation between the initial asymmetry in coordinate space, measured by ϵ_n , and the final asymmetry in momentum space given by $\langle v_n \rangle$. We have found that larger is the collision energy larger is the degree of correlation between ϵ_n and $\langle v_n \rangle$. At LHC there is significantly more correlation than at RHIC. For both collision energies considered and in all the range of impact parameter studied the v_2 is strongly correlated with the ϵ_2 with the linear correlation coefficient $C(2, 2) \approx 0.95$. The degree of correlation between ϵ_n and the corresponding $\langle v_n \rangle$ decrease for higher harmonics. Moreover, in ultra-central collisions we found that $C(n, n) > 0.9$ for $n = 2, 3$ and 4 which imply that the $v_n \propto \epsilon_n$ and they carry out the information about the initial geometry of the fireball. These results joined with the fact that in ultra central collisions the $v_n(p_T)$ have a large sensitivity to the η/s ratio strongly suggest to focus the experimental effort to these collision centrality where it is possible to get better constraint on the value of η/s in the QGP phase and having a new insight on the initial state fluctuations.

VII. ACKNOWLEDGMENTS

V.Greco, S. Plumari, F. Scardina and G.L. Guardo acknowledge the support of the ERC-StG Grant under the QGPDyn project.

References

-
- [1] J. Adams et al. (STAR Collaboration), Nucl.Phys. **A757**, 102 (2005), nucl-ex/0501009.
 - [2] K. Aamodt et al. (ALICE Collaboration), Phys.Rev.Lett. **105**, 252302 (2010), 1011.3914.
 - [3] P. Romatschke and U. Romatschke, Phys.Rev.Lett. **99**, 172301 (2007), 0706.1522.
 - [4] H. Song and U. W. Heinz, Phys.Rev. **C78**, 024902 (2008), 0805.1756.
 - [5] G. Ferini, M. Colonna, M. Di Toro, and V. Greco, Phys.Lett. **B670**, 325 (2009), 0805.4814.
 - [6] Z. Xu and C. Greiner, Phys.Rev. **C79**, 014904 (2009), 0811.2940.
 - [7] S. Plumari and V. Greco, AIP Conf.Proc. **1422**, 56 (2012), 1110.2383.
 - [8] P. Kovtun, D. Son, and A. Starinets, Phys.Rev.Lett. **94**, 111601 (2005), hep-th/0405231.
 - [9] A. Adare et al. (PHENIX Collaboration), Phys.Rev.Lett. **107**, 252301 (2011), 1105.3928.

- [10] E. Richardson (PHENIX Collaboration), PoS **QNP2012**, 146 (2012), 1206.3501.
- [11] G. Aad et al. (ATLAS), Phys. Rev. **C86**, 014907 (2012), 1203.3087.
- [12] H. Petersen, G.-Y. Qin, S. A. Bass, and B. Muller, Phys.Rev. **C82**, 041901 (2010), 1008.0625.
- [13] G.-Y. Qin, H. Petersen, S. A. Bass, and B. Muller, Phys.Rev. **C82**, 064903 (2010), 1009.1847.
- [14] H. Holopainen, H. Niemi, and K. J. Eskola, Phys.Rev. **C83**, 034901 (2011), 1007.0368.
- [15] B. Schenke, S. Jeon, and C. Gale, Phys.Rev. **C85**, 024901 (2012), 1109.6289.
- [16] C. Gale, S. Jeon, B. Schenke, P. Tribedy, and R. Venugopalan, Phys.Rev.Lett. **110**, 012302 (2013), 1209.6330.
- [17] L. Bravina, B. Brusheim Johansson, G. K. Eyyubova, V. Korotkikh, I. Lokhtin, et al., Eur.Phys.J. **C74**, 2807 (2014), 1311.7054.
- [18] B. Abelev et al. (ALICE), Phys. Lett. **B719**, 18 (2013), 1205.5761.
- [19] S. Chatrchyan et al. (CMS), JHEP **02**, 088 (2014), 1312.1845.
- [20] L. P. Csernai, J. Kapusta, and L. D. McLerran, Phys.Rev.Lett. **97**, 152303 (2006), nucl-th/0604032.
- [21] R. A. Lacey, N. Ajitanand, J. Alexander, P. Chung, W. Holzmann, et al., Phys.Rev.Lett. **98**, 092301 (2007), nucl-ex/0609025.
- [22] S. Plumari, V. Greco, and L. Csernai (2013), 1304.6566.
- [23] S. Plumari, V. Greco, and L. Csernai, Nuovo Cim. **C037**, 68 (2014).
- [24] M. Prakash, M. Prakash, R. Venugopalan, and G. Welke, Phys.Rept. **227**, 321 (1993).
- [25] J.-W. Chen, Y.-H. Li, Y.-F. Liu, and E. Nakano, Phys.Rev. **D76**, 114011 (2007), hep-ph/0703230.
- [26] H. B. Meyer, Phys.Rev. **D76**, 101701 (2007), 0704.1801.
- [27] S. K. Das and J.-e. Alam, Phys.Rev. **D83**, 114011 (2011), 1011.4181.
- [28] S. Plumari, W. M. Alberico, V. Greco, and C. Ratti, Phys.Rev. **D84**, 094004 (2011), 1103.5611.
- [29] A. Nakamura and S. Sakai, Phys.Rev.Lett. **94**, 072305 (2005), hep-lat/0406009.
- [30] S. Plumari, A. Puglisi, M. Colonna, F. Scardina, and V. Greco, J.Phys.Conf.Ser. **420**, 012029 (2013), 1209.0601.
- [31] S. Plumari, A. Puglisi, F. Scardina, and V. Greco, Phys.Rev. **C86**, 054902 (2012), 1208.0481.
- [32] M. Ruggieri, F. Scardina, S. Plumari, and V. Greco, Phys.Lett. **B727**, 177 (2013), 1303.3178.
- [33] M. Ruggieri, F. Scardina, S. Plumari, and V. Greco, Phys.Rev. **C89**, 054914 (2014), 1312.6060.
- [34] Z. Xu and C. Greiner, Phys.Rev. **C71**, 064901 (2005), hep-ph/0406278.
- [35] S. Plumari, G. L. Guardo, V. Greco, and J.-Y. Ollitrault, Nucl. Phys. **A941**, 87 (2015), 1502.04066.
- [36] B. Zhang, M. Gyulassy, and C. M. Ko, Phys.Lett. **B455**, 45 (1999), nucl-th/9902016.
- [37] D. Molnar and M. Gyulassy, Nucl.Phys. **A697**, 495 (2002), nucl-th/0104073.
- [38] V. Greco, M. Colonna, M. Di Toro, and G. Ferini, Prog.Part.Nucl.Phys. (2008), 0811.3170.
- [39] S. Plumari, V. Baran, M. Di Toro, G. Ferini, and V. Greco, Phys.Lett. **B689**, 18 (2010), 1001.2736.
- [40] N. Demir and S. A. Bass, Phys.Rev.Lett. **102**, 172302 (2009), 0812.2422.
- [41] V. Greco, C. Ko, and P. Levai, Phys.Rev.Lett. **90**, 202302 (2003), nucl-th/0301093.
- [42] V. Greco, C. Ko, and P. Levai, Phys.Rev. **C68**, 034904 (2003), nucl-th/0305024.
- [43] B. H. Alver, C. Gombeaud, M. Luzum, and J.-Y. Ollitrault, Phys.Rev. **C82**, 034913 (2010), 1007.5469.
- [44] C. Gombeaud and J.-Y. Ollitrault, Phys.Rev. **C77**, 054904 (2008), nucl-th/0702075.
- [45] H. Niemi, G. Denicol, P. Huovinen, E. Molnar, and D. Rischke, Phys.Rev. **C86**, 014909 (2012), 1203.2452.
- [46] Y. Hatta, J. Noronha, G. Torrieri, and B.-W. Xiao, Phys.Rev. **D90**, 074026 (2014), 1407.5952.
- [47] F. G. Gardim, F. Grassi, M. Luzum, and J.-Y. Ollitrault, Phys.Rev. **C85**, 024908 (2012), 1111.6538.
- [48] A. Chaudhuri, M. R. Haque, V. Roy, and B. Mohanty, Phys.Rev. **C87**, 034907 (2013), 1211.2040.
- [49] H. Niemi, G. Denicol, H. Holopainen, and P. Huovinen, Phys.Rev. **C87**, 054901 (2013), 1212.1008.
- [50] G. Aad et al. (ATLAS Collaboration), JHEP **1311**, 183 (2013), 1305.2942.